Combined IASI-NG and MWS Observations for the Retrieval of Cloud Liquid and Ice Water Path: A Deep Learning Artificial Intelligence Approach

Pietro Mastro ⓘ, *Student Member, IEEE*, Guido Masiello ⓘ, Carmine Serio ⓘ, Domenico Cimini ⓘ, Elisabetta Ricciardelli, Francesco Di Paola ⓘ, Tim Hultberg, Thomas August ⓘ, and Filomena Romano ⓘ

Abstract—A neural network (NN) approach is proposed to combine future infrared (IASI-NG) and microwave (MWS) observations to retrieve cloud liquid and ice water path. The methodology is applied to simulated IASI-NG and MWS observations in the period January–October 2019. IASI-NG and MWS observations are simulated globally at synoptic hours (00:00, 06:00, 12:00, 18:00 UTC) and on a regular spatial grid ($0.125° \times 0.125°$) from ECMWF 5-generation reanalysis (ERA5). The state-of-the-art σ-IASI and RTTOV radiative transfer codes are used to simulate IASI-NG and MWS observations, respectively, from the earth's state vector given by ERA5. A principal component analysis of the simulated IASI-NG observations is performed. Accordingly, a NN is developed to retrieve cloud liquid and ice water path from a combination of 24 MWS channels and 30 IASI-NG PCs. Validation indicates that this combination results in liquid and ice water path retrievals with overall accuracy of 1.85 10^{-2} kg/m^2 and 1.18 10^{-2} kg/m^2, respectively, and 0.97 correlation with respect to reference values. The root-mean-square error (RMSE) for CLWP results in about 30% of the mean value (5.91 10^{-2} kg/m^2) and 22% of the variability (1-sigma). Similarly, the RMSE for CIWP results in about 41% of the mean value (2.91 10^{-2} kg/m^2) and 22% of the variability. Two more NN are developed, retrieving cloud liquid and ice water path from microwave observations only (24 MWS channels) and infrared observations only (30 IASI-NG PCs), demonstrating quantitatively the advantage of using the combination of infrared and microwave observations with respect to either one alone.

Index Terms—Artificial neural networks, Fourier transform infrared, low earth orbit satellites, microwave radiometry.

I. INTRODUCTION

CLOUDS are very important regulators of the hydrological and energy cycles of earth. Thus, clouds play a crucial role in Earth's climate, and their sensitivity and feedback are major sources of uncertainty in climate predictions [1]. Cloud physical properties, such as cloud ice water path (CIWP) and cloud liquid water path (CLWP), are among the essential climate variables defined in the framework of the Global Climate Observing System [WMO, 2011]. The last few decades witnessed an increasing trend in cloud observing capabilities, now providing more than 25 years of adequate climate data records from visible, infrared (IR), and microwave (MW) observations [Dowell *et al.*, 2013]. However, the physical characterization of clouds is still challenging. One way to overcome some of the observing limitations is sensor synergy, i.e., combining the complementary advantages offered by different parts of the spectrum [2]–[4]. For example, passive MW observations are sensitive to atmospheric temperature, humidity, and liquid/ice water within the observed volume. In this context, considering the semitransparency of clouds and the increase of liquid water contribution in the emitted signal with higher frequency, microwave radiometers are the most common single-instrument approach to retrieve a large dynamic range of CLWP without saturation. Information on atmospheric water vapor and cloud liquid water can be derived from channels at 23.8, 31.4, 90, and 183 GHz. Information on ice clouds and precipitation can be derived from millimeter wave measurements at 90 and 150 GHz and possibly higher frequency window channels. Similarly, passive IR observations are sensitive to atmospheric temperature, humidity, and liquid/ice clouds as well as some trace gases within the observed volume. Since the early years of satellite meteorology, methods for deriving cloud properties from IR observations have been developed [5]–[7], followed by the development of methods for inferring cloud microphysics, such as cloud particle size and optical thickness [8]–[12]. Hydrometeors forming clouds strongly absorb at IR wavelengths and the IR radiation reaching a spaceborne radiometer is mostly generated close to the cloud top. Conversely, MW radiation emitted from the earth surface is only slightly affected when passing through nonprecipitating clouds. MW are also complementary to IR because MW radiation is sensitive to larger ice crystals and content whereas IR radiation is more sensitive to smaller particles and cirrus clouds with lower ice content. Therefore, a proper combination of IR and MW multispectral measurements may be beneficial for determining the cloud water content, particularly in case of overlapping cloud layers.

Pietro Mastro, Guido Masiello, and Carmine Serio are with the School of Engineering, University of Basilicata, 85100 Potenza, Italy (e-mail: pietro.mastro@unibas.it; guido.masiello@unibas.it; carmine.serio@unibas.it).

Domenico Cimini, Elisabetta Ricciardelli, Francesco Di Paola, and Filomena Romano are with the Institute of Methodologies for Environmental Analysis, Italian National Research Council, 85050 Tito Scalo, Italy (e-mail: domenico.cimini@imaa.cnr.it; elisabetta.ricciardelli@imaa.cnr.it; francesco.dipaola@imaa.cnr.it; filomena.romano@imaa.cnr.it).

Tim Hultberg and Thomas August are with the European Organisation for the Exploitation of Metereological Satellites, 64297 Darmstadt, Germany (e-mail: tim.hultberg@eumetsat.int; thomas.august@eumetsat.int).

As earth observation programs develop, improvements in spatial and spectral resolutions of satellite-borne sensors promote more sophisticated retrieval procedures to estimate cloud products with enhanced accuracy. The upcoming launch of new advanced high spatial and spectral resolution satellite sensors offers the opportunity for more accurate estimates of cloud microphysical parameters, e.g., the next generation atmospheric sounding interferometer (IASI-NG), and the Microwave Sounder (MWS) that will fly from 2024 onwards. Among the prelaunch activities, the European Organization for the Exploitation of Meteorological Satellites (EUMETSAT) funds studies to investigate new retrieval algorithms, including one focusing on cloud physical properties combining MWS and IASI-NG observations, named ComboCloud.

Methods to derive CLWP and CIWP from combined IR and MW observations have been reported using physical and/or regression approaches [13]–[15]. Here, we propose a method exploiting artificial neural networks (NN). NN have been increasingly applied to remote sensing [16]–[18] because they are well adapted to find nonlinear statistical relationships between target and input variables, such as those arising in the satellite remote sensing of geophysical parameters through spectral radiances. One important aspect of NN is its property of serving as a universal approximator [19], thus being able to handle much more complex problems than least square regression, and thus making NNs more suitable to tackle the global scale variability. To this aim, this article investigates the potential of NN to make a supervised regression of CLWP and CIWP contents with the combined use of simulated IASI-NG and MWS measurements in the IR and MW bands.

The rest of this article is organized as follows. Details about the simulated dataset are given in Section II. The methodology is presented in Section III, including information about the machine learning framework and the selection of IASI-NG and MWS channels. Section IV presents the performances of the methodology, quantifying the accuracy and the value of IR-MW combination. Finally, Section V concludes this article.

II. INSTRUMENTS AND DATASETS

This section provides details on the IASI-NG and MWS sensors, and the generation of the simulated spectral dataset used in this article.

A. IASI-NG and MWS Instruments

Following the success of the EUMETSAT Earth Polar System (EPS) program [20], the EPS Second Generation (EPS-SG) program will launch several satellites starting from 2024. The Meteorological Operational SG (MetOp-SG) satellite missions will carry several instruments, with the intent to support and improve current Numerical Weather Prediction at regional and global scales. The first satellite (MetOp-SG-A1), to be launched on 2024, will carry both IASI-NG and MWS, in a sun-synchronous polar orbit at 835 km altitude.

The IASI-NG sensor [21] will represent the key element sensor for the atmospheric observation of the earth system from space and its main objective is to provide suitable information

TABLE I
IASI-NG TECHNICAL CHARACTERISTICS

Characteristic	IASI-NG
Spectral Coverage	continuous in $645\ cm^{-1} - 2760\ cm^{-1}$ range
Spectral Sensing	$0.125\ cm^{-1}$, 16921 channels
Acquisition angles	±46.5°
Sounding Point Density	25 km × 25 km
Nadir Instantaneous Field of View (IFOV)	12 km diameter
Swath width	ca. 2000 km
Nadir IFOV shape	Circular

TABLE II
MWS TECHNICAL CHARACTERISTIC

Characteristic	MWS
Spectral Coverage	not-continuous in 23.8 GHz – 229.0 GHz range
Spectral Sensing	24 Channels
Acquisition angles	±49°
Polarisation	QH and QV
Nadir Instantaneous Field of View (IFOV)	17-40 km diameter
Swath width	ca. 2200 km
Nadir IFOV shape	Circular

on temperature and water vapor profiles, with high accuracy (about 1K) at a vertical resolution in the lower troposphere of about 1km. The instrument is a Michelson interferometer able to measure infrared radiation emitted from the earth, spanning the spectral range W = $645\ \mathrm{cm}^{-1} - 2760\ \mathrm{cm}^{-1}$, with a spectral resolution of $0.25\ \mathrm{cm}^{-1}$ (apodized) and sampling of $\Delta_\sigma = 0.125\ \mathrm{cm}^{-1}$ (see Table I). This results in a number of linearly independent measurable spectral samples or channels equal to $\frac{W}{\Delta_\sigma} + 1 = 16921$.

IASI-NG is a cross-track scanner, with 14 fields of regard (FOR) per scan, spanning an OFF-nadir angle range of $\pm 46.5°$, from left to right in each swath. Each FOR measures a 4×4 array of so-called instantaneous field of view (IFOV), each of which has a ground diameter of 12 km at nadir and 823 km satellite altitude. The distance between FOVs within a given FOR is around 23.83 km at nadir.

The MWS is a passive microwave radiometer at the core of the future EPS-SG mission. MWS has a direct heritage from the Advanced Microwave Sounding Unit A (AMSU-A) and the microwave humidity sounder, currently flying on EUMETSAT MetOp satellites, but with enhanced spectral characteristic with respect to its predecessors, adding two temperature and two humidity sounding channels, plus one high-frequency window channel sensitive to ice clouds. The sensor will operate a total of 24 channels from 23–229 GHz, with a spatial sampling at nadir of about 17–40 km, depending upon channel (see Table II). The primary purposes of MWS are atmospheric temperature and water vapour sounding, as well as CIWP estimates.
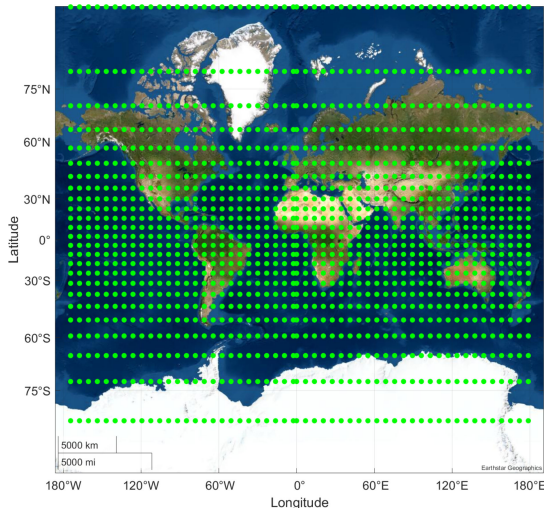
Fig. 1. Map of geographical coordinates of IASI-NG and MWS simulated measurements.

B. Simulated Datasets

IASI-NG and MWS measurements are not available until the launch of EPS-SG-A1 in 2024. Thus, for this article synthetic observations are simulated with the state of art $\sigma - $ IASI [22] and RTTOV [23] radiative transfer codes. The atmospheric state vectors needed for the radiative transfer calculations are taken from ERA5, the fifth generation ECMWF global reanalysis. Four representative days (1st of January, April, July, October 2019), each at four synoptic hours (00, 06, 12, 18), are selected to capture both seasonal and daily cycles at global scale. ERA5 state vectors are provided globally on a regular spatial grid $0.125° \times 0.125°$. However, for our purpose data were decimated by resampling with a latitude/longitude sampling step of $6.875°$, resulting in 53 latitudes and 26 longitudes (see Fig. 1) from $-86.875°$ to $85°$ and from $0°$ to $357.5°$, respectively. This sampling has been chosen for reducing the dataset to a manageable size while retaining the global coverage and the temporal span (4 seasons and 4 synoptic hours). The atmospheric state vector consists of temperature, water vapour, and ozone *(T, Q, O)* profiles along with profiles of specific cloud liquid content, specific cloud ice content, specific rain, and snow water contents. Note that ERA5 provides only large-scale precipitation profiles. This sets a limitation to the applicability of the current set-up to nonconvective systems only. All atmospheric profiles are given on a pressure grid of 37 levels spanning the range 10–1000 hPa. In addition, the surface temperature is also taken from ERA5. Other trace gas profiles are set by climatology.

Three vertical zenith angles (VZA), specifically $0°$, $20°$, and $44°$ have been used to compute the spectral radiances. So, this means that for each VZA a number of simulated soundings equal to $4(\text{days}) \times 4(\text{synopthic hours}) \times 53(\text{latitudes}) \times 26 \ (\text{longitudes}) = 22048$ is considered, resulting in 66144 samples in total. Simulations are performed considering a pencil beam and pass-band computations.

Concerning the surface emissivity, the Masuda model [24] is adopted for the IR simulations, while for the MW simulations

the ocean emissivity is given by the FASTEM model embedded in RTTOV [23]. Recommended RTTOV-SCATT optical properties have been used [25] including Mie spheres for rain and nonprecipitating hydrometeors and sector snowflakes for solid precipitation. For the IR, the all-sky version of σ-IASI (σ-IASI_as) is used [26], [27], which exploits the Chou scaling approximation [28]. The optical properties for ice are those for ice cloud crystal habits aggregates and are taken from the LBLDIS [29] library. LBLDIS library and datasets was used also for liquid water (see [29] for more details).

Simulated observations do include the radiometric noise expected for both instruments. For IASI-NG the spectral radiance is correlated along the wavenumber because of Gaussian apodization.[1] The current radiometric noise requirement for IASI-NG is two times lower than that of IASI instrument. Thus, we assumed level 1B IASI-NG noise equal to half of that of IASI. Noise for level 1C is obtained by the level 1B after Gaussian apodization. If S_ε denotes the level 1C noise covariance matrix of IASI-NG, then the observations are simulated based on the signal-noise additive model according to

$$\boldsymbol{R} = \boldsymbol{r} + \boldsymbol{S}_\varepsilon^{\frac{1}{2}} \boldsymbol{\eta} \qquad (1)$$

where $\boldsymbol{R}$ is the vector (size $N = 16921$) of simulated spectral radiances; $\boldsymbol{r}$ (same size as $\boldsymbol{R}$) is the signal computed according to the forward model; $\boldsymbol{\eta}$ is vector-valued (same size as $\boldsymbol{R}$) of Gaussian noise sample with zero mean and unit variance. Note that the $\boldsymbol{S}_\varepsilon$ matrix (size N×N) includes Gaussian apodization according to IASI-NG specification.

Similarly, for MWS we considered the radiometric noise requirements provided through the WMO Observing Systems Capability Analysis and Review (Oscar) tool.[2] The covariance matrix $\boldsymbol{S}_\varepsilon$ is assumed to be diagonal although for MWS channels.

Finally, the dataset has been partitioned in three different subsets: 1) training, 2) validation, and 3) test dataset. The training and the validation datasets are used to learn and assess the performance of the NN models. The test dataset is used for a final evaluation of the generalization performances of the network to new input data. Specifically, we divided the total dataset as follows: 70% for training, 20% for validation, and 10% for test.

III. METHODOLOGY

This section describes the proposed retrieval scheme. First, we present the NN regression framework, and then we introduce the analysis related to the preprocessing of IASI-NG and MWS observations.

A. NN Regression Framework

Multilayer perceptron (MLP) [30], [31] is nowadays the leading architecture used for implementing NN supervised regressors. From a set of samples $\mathbb{S}(X, y)$, where X represents the set of inputs and y the corresponding outputs, MLP emulates a

---

neural structure, linking many parallel processors called "perceptrons" to map $X \rightarrow y$. These processors are organized in distinct layers: 1) the first layer represents the set of network inputs X, 2) the last layer represents the output of the mapping $X \rightarrow y$, and 3) a number of intermediate layers, also called "hidden layers". The entire neuronal structure is connected via perceptron links associated with network weights W. The ensemble of perceptrons, links, and weights, provides to the NN architecture the ability to learn from example and make predictions. The learning is pursued by the adoption of forward- and backward-propagation algorithms whose objective is to minimize the error between NN predictions and training outputs. Keras-python framework [32] has been used to build and implement the NN structure. To this end, Keras offers a built-in tuner [33] to optimize the searching for the best NN structure with respect to the input/output units and a set of "hyperparameters" (e.g., the number of hidden layers, hidden units, activation function, optimizer, and so on). In this article, the Bayesian tuner [34], [35] has been used. Based on random selection, Bayesian tuner addresses the problem of finding the best NN architecture for a given learning task and dataset. The search for the best hyperparameters is based on network morphism in NN architecture search [34] and a tree-structure search space [36].

B. IASI-NG and MWS Preprocessing

In processing hyperspectral data, such as from IASI-NG, principal component analysis (PCA) [37], [38] is key to reduce the high-dimensionality of the data space. Since it is well established that high-dimensional MLP architectures are more prone to overfit [39], [40], this article exploits PCA to develop a statistical NN regressor with a low-dimensional architecture. A common approach is used to build the IASI-NG PCA basis [37]. First, we consider an ensemble of M state vectors $\boldsymbol{R}$, which are piled up in the columns of the matrix $\boldsymbol{\Sigma}$ (of size $N \times M$, with $M < N$). Only clear sky radiances are considered to build $\boldsymbol{\Sigma}$. Before building $\boldsymbol{\Sigma}$, the radiance vector $\boldsymbol{R}$ is centred by removing the mean and normalized to the IASI-NG covariance matrix

$$\boldsymbol{S}_{\varepsilon}^{-\frac{1}{2}} \left(\boldsymbol{R} - \bar{\boldsymbol{R}} \right) \tag{2}$$

with $\bar{\boldsymbol{R}}$ the mean value of the ensemble. The covariance matrix of the ensemble $\boldsymbol{C}$ is then computed as

$$\boldsymbol{C} = \frac{1}{M} \boldsymbol{\Sigma}\boldsymbol{\Sigma}^{t} \tag{3}$$

where the superscript t denotes the transpose matrix. The basis of eigenvectors $\boldsymbol{U}$, is obtained by singular value decomposition of $\boldsymbol{C}$

$$\boldsymbol{C} = \mathbf{U}\mathbf{S}\mathbf{V}^{t} \tag{4}$$

where $\boldsymbol{S}$ is the diagonal matrix of singular values, and $\mathbf{U} = \mathbf{V}$ the basis of eigenvectors. Note that all matrices have size $N \times N$, and $\mathbf{U} = \mathbf{V}$, because the matrix C is symmetric. For a given radiance vector $\boldsymbol{R}$ (clear or cloudy), the vector of principal component coefficients (or scores vector) $\boldsymbol{c}$ is obtained according to

$$\boldsymbol{c} = \boldsymbol{U} \left(\boldsymbol{S}_{\varepsilon}^{-\frac{1}{2}} \left(\boldsymbol{R} - \bar{\boldsymbol{R}} \right) \right). \tag{5}$$

Conversely, the 24 MWS channels are used directly as input to the NN.

C. Neural Network Training Process

Using the Bayesian tuner, a NN structure composed of 5 layers was designed. The input layer is composed by 55 input units, i.e., the first 30 IASI PCs, 24 MWS channels, and the VZA. A criterium for selecting IASI PCs is suggested in [37], where they demonstrate that the number of IASI-PC that would separate the signal from noise ranges between 10–100. Thus, to be conservative we select 30 IASI-PC for the retrieval process, which span 99.96% of the total variance. The dataset was preliminarily filtered to avoid extremely large CLWP/CIWP values (i.e., CLWP and CIWP larger than 0.6 kg/m² and 0.5 kg/m², respectively) that may harm the NN training, screening out less than 0.3% of the initial dataset. In addition, to avoid uncertainty due to surface emissivity in the MW spectral region, only simulations over ocean are considered in this analysis. These two screenings leave 31593 samples in total, which are then divided in three sets used to train (70% = 22746 samples), validate (20% = 5687 samples), and test (10% = 3160 samples) the NN model. The partitioning of the samples into training, validation, and test datasets was such to keep the same variability with respect to the VZA parameter. Because the dynamic range of IASI-NG PCA and MWS brightness temperatures may greatly differ, it is good practice to normalize the two data spaces. This is achieved by means of standard normalization (i.e., inputs are normalized with respect to the training set by removing the mean and scaling to unit variance), applied to both IASI-NG PCs and MWS channels. Three hidden layers, composed, respectively, of 1024, 1024, and 64 hidden units are chosen by the tuner. The output layer is composed by two units corresponding to CLWP and CIWP. The ReLU [41] function is used to activate the network units, and the mean squared error (MSE) is used as the loss function

$$\mathrm{MSE} = \frac{1}{N_S} \sum_{i=0}^{N_S - 1} \left(y_i - \hat{y}_i \right)^2 \tag{6}$$

where $\hat{y}_i$ is the predicted value of the ith corresponding output true value y_i; N_S indicates the total number of samples to predict. The NN learning step is based on a backpropagation algorithm, whose goal is to update the NN learning parameters [31], minimizing a loss function at each temporal iteration (epoch), and ideally finding its global minimum. In literature this process is indicated as optimization task and is handled by a specific algorithm. In this article, we adopted an "adaptive momentum" based optimizator, specifically the Adam algorithm [42], regularized according to the weight decay algorithm [43]. Adam is a mini-batch optimization algorithm, representing nowadays the de facto standard to train deep learning NN models [30], due to its high versatility in adapting to complex architectures with high capacity cost functions [44]. Table III displays a summary of the NN parameters used in this article.

The tuner indicates as optimal architecture a multilayer NN. With limited training data, however, this complex architecture

TABLE III
SUMMARY OF NN PARAMETERS FOR THE COMBINED IR-MW CONFIGURATION
DEVELOPED IN THIS ARTICLE (INDICATED AS M1 IN FIGS. 4 AND 6)

N. layers	5
N. hidden layers	3
N. input units	55 (30 IASI-NG PCs + 24 MWS Channels + VZA)
N. hidden units of the hidden layer 1	1024
N. hidden units of the hidden layer 2	1024
N. hidden units of the hidden layer 3	64
N. output units	2 (CLWP and CIWP)
Units activation function	ReLU
Optimization algorithm	Adam [42]
Implicit regularization	Early stopping [30]
Explicit regularization	Weight decay [43]
NN architecture finder	Bayesian tuner [35], [36]
Loss function	MSE

TABLE IV
SUMMARY OF NN PARAMETERS FOR THE MW-ONLY CONFIGURATION
(INDICATED AS M2 IN FIGS. 4 AND 6)

N. layers	5
N. hidden layers	3
N. input units	25 (24 MWS Channels + VZA)
N. hidden units of the hidden layer 1	64
N. hidden units of the hidden layer 2	32
N. hidden units of the hidden layer 3	64
N. output units	2 (CLWP and CIWP)
Units activation function	ReLU
Optimization algorithm	Adam [42]
Implicit regularization	Early stopping [30]
Explicit regularization	Weight decay [43]
NN architecture finder	Bayesian tuner [35], [36]
Loss function	MSE

Fig. 2. Neural network training and validation loss function history.

TABLE V
SUMMARY OF NN PARAMETERS FOR THE IR-ONLY CONFIGURATION
(INDICATED AS M3 IN FIGS. 4 AND 6)

N. layers	5
N. hidden layers	3
N. input units	31 (30 IASI-NG PCs + VZA)
N. hidden units of the hidden layer 1	1024
N. hidden units of the hidden layer 2	256
N. hidden units of the hidden layer 3	32
N. output units	2 (CLWP and CIWP)
Units activation function	ReLU
Optimization algorithm	Adam [42]
Implicit regularization	Early stopping [30]
Explicit regularization	Weight decay [43]
NN architecture finder	Bayesian tuner [35], [36]
Loss function	MSE

could lead to overfitting; for this reason we adopted regularization, aiming at making the model generalize better, i.e., produce better results on the test set [45]. The use of regularization to avoid overfitting has been proved empirically [30]. In fact, there are many worked examples in the open literature showing how high-capacity architectures, i.e., NN with more parameters than training data couples, can improve the generalization performance. In other words, contrarily to overfitted architectures, the validation error remains close to the training one. This empirical evidence has been rigorously proved in mathematical form by [44]. In effect, Belkin *et al.* [44] demonstrated that the deep learning architecture is the condition needed to move beyond the classical under-parameterized regime to the modern interpolation where the predictors have negligible training risk.

Since we move to the interpolating regime, in this article, we dedicate particular care to the training, validation, and test steps of the NN. The NN model has been trained and validated for 100 epochs on the dataset of MWS + IASI-NG measurements indicated in Section II. Fig. 2 reports the NN learning performances

in training and validation steps, showing that the validation error is stable and follows the training error.

To demonstrate the value of MW and IR combination, we also developed two reference NN architectures, based respectively on IASI-NG only and MWS only. By comparing the performances of the three different configurations, the advantage of combining IR and MW with respect to either one can be quantified. For MW-only, the NN configuration takes in input the VZA and the 24 MWS channels. For IR-only, the configuration takes in input the VZA and the first 30 IASI-NG PCs. Similarly to the IR-MW combined architecture, the MW-only and IR-only NN configurations are optimized by the tuner, as reported in Tables IV and V. The three architectures are hereafter indicated
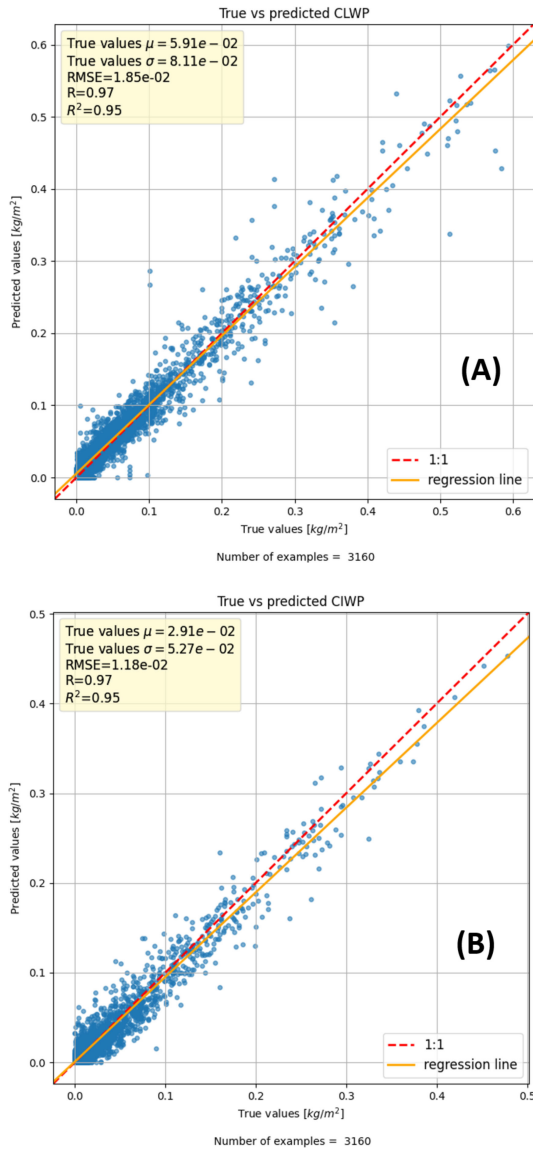
Fig. 3. Scatterplot of the NN prediction for CLWP (A) and CIWP (B). These results correspond to the M1 configuration, taking in input the combination of IASI-NG & MWS observations. μ and σ indicate the mean and std of the reference true values. Except for correlation and determination coefficients (R and R^2), units are in kg/m^2.
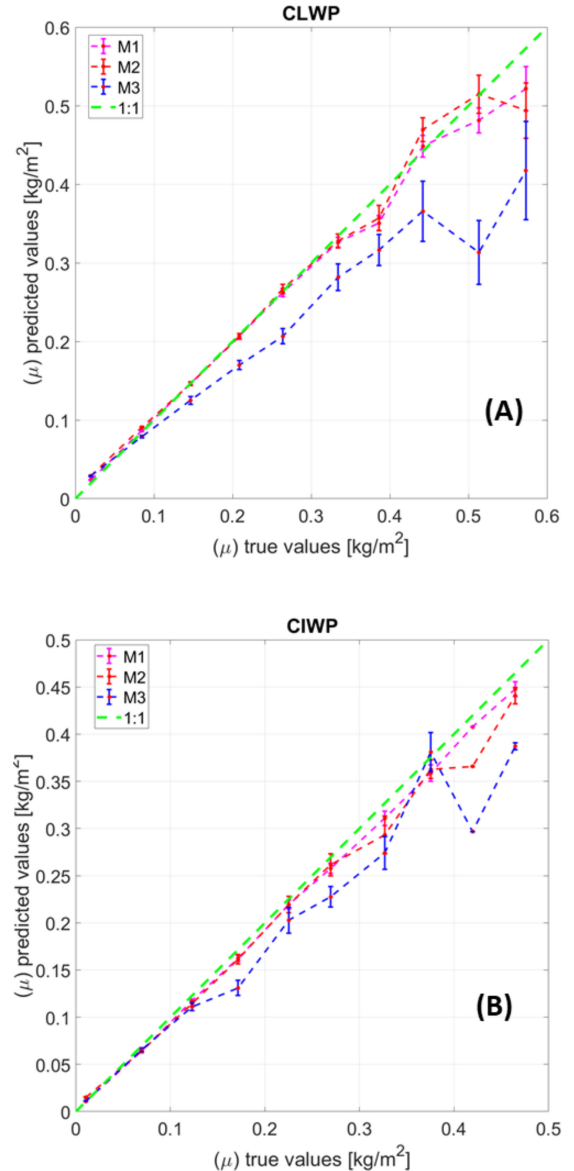

Fig. 4. Error analysis of the NN to estimate CLWP (A) and CIWP (B). The figure shows the mean of predicted values as a function of true ones. The errorbars indicate the uncertainty corresponding to each binned estimate.

as M1 (combined IASI-NG and MWS), M2 (MWS), and M3 (IASI-NG).

IV. RESULTS

This section analyses the performances of the NN configurations introduced in Section III-C. A quantitative intercomparison of M1, M2, and M3 is also shown.

As anticipated in Section II, after the NN learning process the regression performances are tested on a set of unseen simulated measurements.

The results are shown in Fig. 3, indicating a good capability to infer both CLWP and CIWP from the combination of the MW and IR observations. The overall root-mean-square error (RMSE) for CLWP is 1.85×10^{-2} kg/m^2, while 1.18×10^{-2}

kg/m^2 for CIWP. The RMSE for CLWP results in about 30% of the mean value and 22% of the variability (1-sigma). Similarly, the RMSE for CIWP results in about 41% of the mean value and 22% of the variability. These results are comparable with, though better than, previously reported, e.g., [46] using third-order multiple regression and maximum likelihood algorithms to retrieve CLWP and CIWP from a simulated dataset of MW observations at a subset of MWS channels.

To further assess the performance of the M1 configuration, and to compare it with M2 and M3, we performed a binning analysis of the scatter plots such as in Fig. 3. For this aim, the x-axis is divided in ten bins; for each bin the average and standard deviation of true and the corresponding predicted values are computed. These are displayed in Fig. 4, for both CLWP and CIWP and all the three configurations, providing information
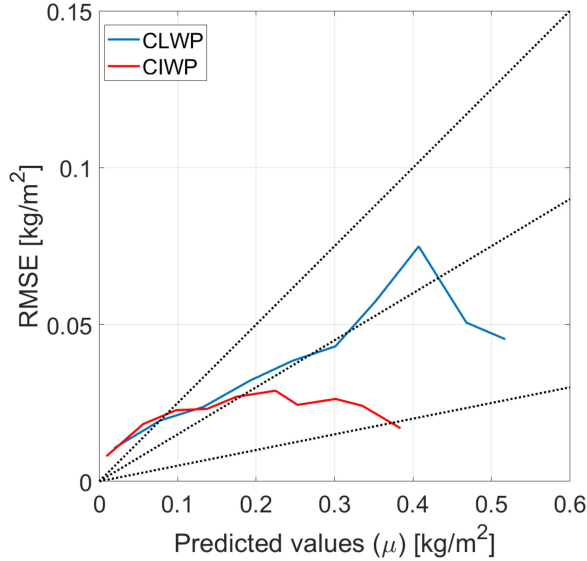
Fig. 5. Root-mean-square error of the estimate of CLWP and CIWP obtained from the NN approach. The three dotted lines correspond to 5% (lower), 15% (middle), and 25% (higher) error. Results for the M1 configuration (MWS+IASI-NG combination) are shown.

on systematic and random error as a function of the absolute values. Fig. 4 helps picturing the contribution of the IR and MW observations to the combined approach.

Some comments may be derived from Fig. 4. For CLWP it is seen that M3 (IASI-NG) yields unbiased values only for small values (<0.1 kg/m^2). The reason is that IASI-NG radiances soon saturate in presence of thicker water clouds. In contrast, MWS predictions are fairly unbiased up to the value of $\cong 0.30$ kg/m^2. As expected, the MW-IR combination provides more information and, thus, predictions are closer to the 1:1 line. Similar comments apply to CIWP. The same binned analysis is used to estimate the RMSE as a function of the predicted values, as shown in Fig. 5. The binned analysis shows that the RMSE tends to increase with the estimated value, staying between 5-25% for both CLWP and CIWP, except for values lower than 0.1 kg/m^2.

To illustrate the value of IR+MW combination with respect to the individual systems (IR- and MW-only), in Fig. 6, we use the Taylor diagram [47]. The Taylor diagram provides a graphical and intuitive method to compare the performances of the three NN configurations to retrieve CLWP and CIWP. The performances are quantified in terms of three statistics: 1) the Pearson correlation coefficient, 2) the RMSE, and 3) the standard deviation. From Fig. 6, the relative merit of the different NN configurations is evident. Concerning CLWP predictions [see Fig. 6(a)], it is straightforward that M1 shows the best retrieval performances. M2 also shows good performances, confirming the ability of MW sensor to infer CLWP, while M3 performances are worst. Similar consideration applies for the CIWP retrieval [see Fig. 6(b)], where the configuration performances are considerably better for M1 than for M2 and M3. Quantitatively, the IR and MW combination (M1) provides CLWP with 2% higher correlation and a 1.4 factor lower RMSE with respect to MW only (M2), and 14% higher correlation and a 2.4 factor lower RMSE with respect to IR only (M3). Concerning CIWP, the
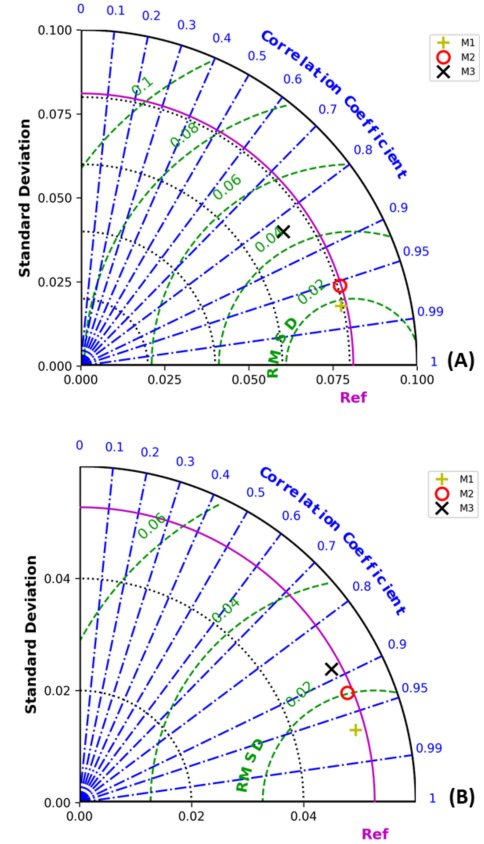

Fig. 6. Taylor diagram analysis for CLWP (A) and CIWP (B). The analysis refers to the three NN architecture, M1, M2, and M3 developed in this article.

TABLE VI
M1, M2, AND M3 PERFORMANCES IN TERMS OF RMSE OF THE CLWP AND CIWP REGRESSION FOR THE TRAINING, VALIDATION, AND TEST DATASETS. UNITS ARE IN 10^{-2} KG/M^2

	CLWP			CIWP		
	Train	**Valid**	**Test**	**Train**	**Valid**	**Test**
M1	0.65	1.85	1.85	0.52	1.34	1.18
M2	2.09	2.59	2.52	1.94	2.09	2.04
M3	1.94	4.65	4.50	1.50	2.42	2.51

IR and MW combination provides 4% higher correlation and a 1.7 factor lower RMSE with respect to MW only, and 8% higher correlation and a 2.1 factor lower RMSE with respect to IR only.

Finally, to demonstrate that our approach, which operates in the interpolating regime, does not lose in terms of generalization, Table VI shows the RMSE computed for the training, validation and test datasets for both CLWP and CIWP and the three configurations. Note that the performances for the validation and test datasets are nearly the same, indicating that a fair generalization has been achieved.

V. CONCLUSION

This article focuses on the potential of a deep learning approach to infer microphysical key cloud parameters (CLWP and CIWP) by the synergic use of IR and MW observations. Results indicate that the combined use of IR and MW modern sensors allow us to estimate CLWP with an overall RMSE of 1.85×10^{-2} kg/m^2. For CIWP, the RMSE is 1.18×10^{-2} kg/m^2. According to

the WMO OSCAR requirements for global NWP applications, the obtained accuracy is close to the breakthrough values (20 and 10 g/m^2, respectively) and about half the threshold values (50 and 20 g/m^2, respectively).[3]

A comparison was carried out to assess the added-value of the combined IR and MW measurements with respect to MW or IR measurements separately. It is shown that the IR and MW combination provides CLWP with higher correlation (2–14%) and lower RMSE (factor of 1.4–2.4) than single MW and IR only, respectively. Similarly, for CIWP, with 4–8% higher correlation and 1.7–2.1 factor lower RMSE, respectively.

Finally, the analysis will be consolidated on the basis of real observations, an effort that is ongoing using IASI and AMSU observations. Nevertheless, the synergy of IR and MW has been proved, paving the road to more complete exploitation of next generation satellite platforms for weather and climate.

REFERENCES

[1] V. Masson-Delmotte, Ed. *et al.*, *Climate Change 2021: The Physical Science Basis. Contribution of Working Group I to the Sixth Assessment Report of the Intergovernmental Panel on Climate Change*. Cambridge, U.K.: Cambridge Univ. Press, 2021.

[2] B. Lin *et al.*, "Estimation of water cloud properties from satellite microwave, infrared and visible measurements in oceanic environments: 2 Results," *J. Geophysical Res., Atmos.*, vol. 103, no. D4, pp. 3887–3905, 1998, doi: 10.1029/97JD02817.

[3] T. T. Wilheit and K. D. Hutchison, "Retrieval of cloud base heights from passive microwave and cloud top temperature data," *IEEE Trans. Geosci. Remote Sens.*, vol. 38, no. 3, pp. 1253–1259, May 2000, doi: 10.1109/36.843017.

[4] F. Chevallier, P. Bauer, J.-F. Mahfouf, and J.-J. Morcrette, "Variational retrieval of cloud profile from ATOVS observations," *Quart. J. Roy. Meteorol. Soc.*, vol. 128, no. 585, pp. 2511–2525, Oct. 2002, doi: 10.1256/qj.01.153.

[5] S. Fritz and J. S. Winston, "Synoptic use of radiation measurements from satellite tiros II," *Monthly Weather Rev.*, vol. 90, no. 1, pp. 1–9, Jan. 1962, doi: 10.1175/1520-0493(1962)090<0001:SUORMF>2.0.CO;2.

[6] W. L. Smith and C. M. R. Platt, "Comparison of satellite-deduced cloud heights with indications from radiosonde and ground-based laser measurements," *J. Appl. Meteorol. Climatol.*, vol. 17, no. 12, pp. 1796–1802, Dec. 1978, doi: 10.1175/1520-0450(1978)017<1796:COSDCH>2.0.CO;2.

[7] W. P. Menzel, W. L. Smith, and T. R. Stewart, "Improved cloud motion wind vector and altitude assignment using VAS," *J. Appl. Meteorol. Climatol.*, vol. 22, no. 3, pp. 377–384, Mar. 1983, doi: 10.1175/1520-0450(1983)022<0377:ICMWVA>2.0.CO;2.

[8] J. R. Eyre and W. P. Menzel, "Retrieval of cloud parameters from satellite sounder data: A simulation study," *J. Appl. Meteorol. Climatol.*, vol. 28, no. 4, pp. 267–275, Apr. 1989, doi: 10.1175/1520-0450(1989)028<0267:ROCPFS>2.0.CO;2.

[9] W. P. Menzel, T. J. Schmit, and D. P. Wylie, "Cloud characteristics over central amazonia during GTE/ABLE 2B derived from multispectral visible and infrared spin scan radiometer atmospheric sounder observations," *J. Geophysical Res., Atmos.*, vol. 95, no. D10, pp. 17039–17042, 1990, doi: 10.1029/JD095iD10p17039.

[10] P. Minnis, K.-N. Liou, and Y. Takano, "Inference of cirrus cloud properties using Satellite-observed visible and infrared radiances. Part I: Parameterization of radiance fields," *J. Atmospheric Sci.*, vol. 50, no. 9, pp. 1279–1304, May 1993, doi: 10.1175/1520-0469(1993)050<1279:IOCCPU>2.0.CO;2.

[11] P. Minnis, P. W. Heck, and D. F. Young, "Inference of cirrus cloud properties using Satellite-observed visible and infrared radiances. Part II: Verification of theoretical cirrus radiative properties," *J. Atmospheric Sci.*, vol. 50, no. 9, pp. 1305–1322, May 1993, doi: 10.1175/1520-0469(1993)050<1305:IOCCPU>2.0.CO;2.

[12] B. H. Kahn *et al.*, "Near micron-sized cirrus cloud particles in high-resolution infrared spectra: An orographic case study," *Geophysical Res. Lett.*, vol. 30, no. 8, 2003, doi: 10.1029/2003GL016909.

[13] J. Huang *et al.*, "Determination of ice water path in ice-over-water cloud systems using combined MODIS and AMSR-E measurements," *Geophysical Res. Lett.*, vol. 33, no. 21, 2006, doi: 10.1029/2006GL027038.

[14] F. Romano, D. Cimini, R. Rizzi, and V. Cuomo, "Multilayered cloud parameters retrievals from combined infrared and microwave satellite observations," *J. Geophysical Res., Atmos.*, vol. 112, no. D8, 2007, doi: 10.1029/2006JD007745.

[15] N. R. Nalli *et al.*, "Validation of satellite sounder environmental data records: Application to the Cross-track infrared microwave sounder suite," *J. Geophysical Res., Atmos.*, vol. 118, no. 24, pp. 13,628–13,643, 2013, doi: 10.1002/2013JD020436.

[16] J. F. Mas and J. J. Flores, "The application of artificial neural networks to the analysis of remotely sensed data," *Int. J. Remote Sens.*, vol. 29, no. 3, pp. 617–663, Feb. 2008, doi: 10.1080/01431160701352154.

[17] J. Holloway and K. Mengersen, "Statistical machine learning methods and remote sensing for sustainable development goals: A review," *Remote Sens.*, vol. 10, no. 9, Sep. 2018, Art. no. 9, doi: 10.3390/rs10091365.

[18] E. S. Maddy and S. A. Boukabara, "MIIDAPS-AI: An explainable machine-learning algorithm for infrared and microwave remote sensing and data assimilation preprocessing - Application to LEO and GEO sensors," *IEEE J. Sel. Topics Appl. Earth Observ. Remote Sens.*, vol. 14, pp. 8566–8576, Aug. 2021, doi: 10.1109/JSTARS.2021.3104389.

[19] K. Hornik, M. Stinchcombe, and H. White, "Multilayer feedforward networks are universal approximators," *Neural Netw.*, vol. 2, no. 5, pp. 359–366, Jan. 1989, doi: 10.1016/0893-6080(89)90020-8.

[20] H. J. Kramer, "Meteorology — GEO (Geosynchronous earth orbit) missions," in *Observation of the Earth and its Environment: Survey of Missions and Sensors*, H. J. Kramer Ed. Berlin, Heidelberg: Springer, 2002, pp. 607–660, doi: 10.1007/978-3-642-56294-5_7.

[21] C. Crevoisier *et al.*, "Towards IASI-New generation (IASI-NG): Impact of improved spectral resolution and radiometric noise on the retrieval of thermodynamic, chemistry and climate variables," *Atmos. Meas. Tech.*, vol. 7, no. 12, pp. 4367–4385, Dec. 2014, doi: 10.5194/amt-7-4367-2014.

[22] U. Amato, G. Masiello, C. Serio, and M. Viggiano, "The σ-IASI code for the calculation of infrared atmospheric radiance and its derivatives," *Environ. Model. Softw.*, vol. 17, no. 7, pp. 651–667, Nov. 2002, doi: 10.1016/S1364-8152(02)00027-0.

[23] R. Saunders *et al.*, "An update on the RTTOV fast radiative transfer model (currently at version 12)," *Geosci. Model Dev.*, vol. 11, no. 7, pp. 2717–2737, Jul. 2018, doi: 10.5194/gmd-11-2717-2018.

[24] K. Masuda, T. Takashima, and Y. Takayama, "Emissivity of pure and sea waters for the model sea surface in the infrared window regions," *Remote Sens. Environ.*, vol. 24, no. 2, pp. 313–329, Mar. 1988, doi: 10.1016/0034-4257(88)90032-6.

[25] A. J. Geer and F. Baordo, "Improved scattering radiative transfer for frozen hydrometeors at microwave frequencies," *Atmospheric Meas. Techn.*, vol. 7, no. 6, pp. 1839–1860, Jun. 2014, doi: 10.5194/amt-7-1839-2014.

[26] G. Liuzzi, G. Masiello, C. Serio, D. Meloni, C. Di Biagio, and P. Formenti, "Consistency of dimensional distributions and refractive indices of desert dust measured over lampedusa with IASI radiances," *Atmospheric Meas. Techn.*, vol. 10, no. 2, pp. 599–615, Feb. 2017, doi: 10.5194/amt-10-599-2017.

[27] M. Martinazzo, D. Magurno, W. Cossich, C. Serio, G. Masiello, and T. Maestri, "Assessment of the accuracy of scaling methods for radiance simulations at far and mid infrared wavelengths," *J. Quantitative Spectrosc. Radiative Transfer*, vol. 271, Sep. 2021, Art. no. 107739, doi: 10.1016/j.jqsrt.2021.107739.

[28] M.-D. Chou, K.-T. Lee, S.-C. Tsay, and Q. Fu, "Parameterization for cloud longwave scattering for use in atmospheric models," *J. Climate*, vol. 12, no. 1, pp. 159–169, Jan. 1999, doi: 10.1175/1520-0442(1999)012<0159:PFCLSF>2.0.CO;2.

[29] D. D. Turner, S. A. Ackerman, B. A. Baum, H. E. Revercomb, and P. Yang, "Cloud phase determination using ground-based AERI observations at SHEBA," *J. Appl. Meteorol.*, no. 6, vol. 42, pp. 701–705, 2003.

[30] I. Goodfellow, Y. Bengio, and A. Courville, *Deep Learning*. Cambridge, MA, USA: MIT Press, 2016.

[31] J. E. Ball, D. T. Anderson, and C. S. Chan, "A comprehensive survey of deep learning in remote sensing: Theories, tools and challenges for the community," *J. Appl. Remote Sens*, vol. 11, no. 4, Sep. 2017, doi: 10.1117/1.JRS.11.042609.

[3][Online]. Available:https://www.wmo-sat.info/oscar/requirements

[32] F. Chollet *et al.*, "Keras," GitHub, 2015. [Online]. Available: https://keras.io/

[33] T. O'Malley *et al.*, "Keras tuner," 2019. [Online]. Available: https://github.com/keras-team/keras-tuner

[34] K. Kandasamy, W. Neiswanger, J. Schneider, B. Póczos, and E. P. Xing, "Neural architecture search with bayesian optimisation and optimal transport," in *Proc. 32nd Int. Conf. Neural Inf. Process. Syst.*, New York, NY, USA, Dec. 2018, pp. 2020–2029.

[35] J. Snoek, H. Larochelle, and R. P. Adams, "Practical bayesian optimization of machine learning algorithms," in *Advances in Neural Information Processing Systems*, vol. 25. Vancouver, USA: NIPS, 2012. Accessed: Aug. 13, 2021. [Online]. Available: https://proceedings.neurips.cc/paper/2012/hash/05311655a15b75fab86956663e1819cd-Abstract.html

[36] H. Jin, Q. Song, and X. Hu, "Auto-Keras: An efficient neural architecture search system," in *Proc. 25th ACM SIGKDD Int. Conf. Knowl. Discov. Data Mining*, New York, NY, USA, Jul. 2019, pp. 1946–1956, doi: 10.1145/3292500.3330648.

[37] C. Serio *et al.*, "PCA determination of the radiometric noise of high spectral resolution infrared observations from spectral residuals: Application to IASI," *J. Quantitative Spectrosc. Radiative Transfer*, vol. 206, pp. 8–21, Feb. 2018, doi: 10.1016/j.jqsrt.2017.10.022.

[38] I. T. Jolliffe and J. Cadima, "Principal component analysis: A review and recent developments," *Philos. Trans. Roy. Soc. A*, vol. 374, no. 2065, Apr. 2016, Art. no. 20150202, doi: 10.1098/rsta.2015.0202.

[39] R. Caruana, S. Lawrence, and C. L. Giles, "Overfitting in neural nets: Backpropagation, conjugate gradient, and early stopping," in *Advances in Neural Information Processing Systems 13*, T. K. Leen, T. G. Dietterich, and V. Tresp, Eds. Cambridge, MA, USA: MIT Press, 2001, pp. 402–408, Accessed: Aug. 13, 2020. [Online]. Available: http://papers.nips.cc/paper/1895-overfitting-in-neural-nets-backpropagation-conjugate-gradient-and-early-stopping.pdf

[40] A. P. Piotrowski and J. J. Napiorkowski, "A comparison of methods to avoid overfitting in neural networks training in the case of catchment runoff modelling," *J. Hydrol.*, vol. 476, pp. 97–111, Jan. 2013, doi: 10.1016/j.jhydrol.2012.10.019.

[41] V. Nair and G. E. Hinton, "Rectified linear units improve restricted boltzmann machines," in *Proc. 27th Int. Conf. Int. Conf. Mach. Learn.*, Madison, WI, USA, Jun. 2010, pp. 807–814.

[42] D. P. Kingma and J. B. Adam, "A method for stochastic," *Optim. ICLR*, vol. 5, 2015.

[43] I. Loshchilov and F. Hutter, "Decoupled weight decay regularization," 2017, doi: 10.48550/ARXIV.1711.05101.

[44] M. Belkin, D. Hsu, S. Ma, and S. Mandal, "Reconciling modern machine-learning practice and the classical bias–variance trade-off," *PNAS*, vol. 116, no. 32, pp. 15849–15854, Aug. 2019, doi: 10.1073/pnas.1903070116.

[45] J. Kukačka, V. Golkov, and D. Cremers, "Regularization for deep learning: A taxonomy," 2017, doi: 10.48550/ARXIV.1710.10686.

[46] F. S. Marzano *et al.*, "Flower constellation of millimeter-wave radiometers for tropospheric monitoring at pseudogeostationary scale," *IEEE Trans. Geosci. Remote Sens.*, vol. 47, no. 9, pp. 3107–3122, Sep. 2009, doi: 10.1109/TGRS.2008.2012349.

[47] K. E. Taylor, "Summarizing multiple aspects of model performance in a single diagram," *J. Geophysical Res., Atmos.*, vol. 106, no. D7, pp. 7183–7192, 2001, doi: 10.1029/2000JD900719.

Pietro Mastro (Student Member, IEEE) received the M.S. degree (*summa cum laude*) in computer engineering and information technology in 2019 from the University of Basilicata, Potenza, Italy, where he is currently working toward the Ph.D. degree in engineering for innovation and sustainable development.

His research activities are about in the field of differential synthetic aperture radar interferometry for the monitoring of surface deformation phenomena induced by subsidence, volcano activities, and earthquakes. His main research interests include the field of remote sensing with active and passive sensors, specifically, in the development of methods in the domain of Fourier spectroscopy, and techniques applied to the study of environment, Earth atmosphere, land processes, and remote sensing of atmospheric and surface parameters.

Dr. Mastro was a recipient of the Central-North Italy Chapter best M.S. degree thesis in Geoscience and Remote Sensing Award from the IEEE Geoscience and Remote Sensing Society in 2019.

Guido Masiello teaches at the School of Engineering, University of Basilicata, Potenza, Italy, where he is currently an Associate Professor of Earth and Atmospheric Physics. He works on applied spectroscopy topics, developing methods and instruments for the retrieval of the thermodynamic state of the Earth's atmosphere. He is a Co-Investigator in various projects in the area of high spectral resolution infrared sounders from satellites (far and thermal, from 100 to 3.5 micron): IASI, the Infrared Atmospheric Sounder Interferometer of the French Space Agency, CNES, and EUMETSAT, REFIR, the Radiation Explorer in the Far Infrared (a three years EU project supported within the 4th framework program), MTG-IRS, the Meteosat Third Generation Infrared Sounder (a joint program ESA/EUMETSAT), IASI-NG, the next generation of IASI (CNES and EU-METSAT).

Mr. Masiello was a Reviewer for several *International Journal of Optics and Journal of the Atmospheric Sciences* and for Italian and international research funding agencies.

Carmine Serio Carmine Serio born in July 9, 1954. He received the degree in physics from the University of Naples, Naples, Italy, in February 1978.

He is currently a Full Professor in Earth physics. He is the Director of the School of Engineering, University of Basilicata, Potenza, Italy, where he teaches environmental and atmospheric physics courses. Since 1990, he has been performing research in the field of Fourier spectroscopy, methods, and experimental techniques, applied to the study of environment, Earth atmosphere, land processes, and remote sensing of atmospheric and surface parameters. His experience with Fourier transform infrared spectrometers, or FTIR instruments, include ground-based, airborne, and satellite platforms. He currently develops cutting-edge forward/inverse models for hyperspectral infrared observations. In addition, he acted as Principal Investigator in various projects in high spectral resolution infrared sounders from satellites. These projects include the interferometric monitoring for greenhouse gases (IMG of the Japanese NASDA), the infrared atmospheric sounder interferometer (IASI of the French Space Agency, CNES, and EUMETSAT), the radiation explorer in the far-infrared (REFIR, a three years EU project supported within the 4th framework program), the Meteosat Third Generation Infrared Sounder (MTG-IRS a joint program ESA/EUMETSAT), IASI-next-generation (IASI-NG of CNES and EUMETSAT). He is a Member of the core science team of the Far-infrared-Outgoing-Radiation Understanding and Monitoring mission. The mission was selected in September 2019 by the ESA board Committee to fly in 2026 as part of the Earth Explorer Mission-9, Earth Observation Envelope Programme. Because of his expertise, he has acted as a reviewer of satellite experiments and projects.

Domenico Cimini received the Laurea *(cum laude)* and Ph.D. degrees in physics from the University of L'Aquila, L'Aquila, Italy.

He is currently a Research Manager with the Institute of Methodologies for Environmental Analysis, Italian National Research Council, Tito Scalo, Italy. Since 2002, he has been a Researcher with the Center of Excellence for Remote Sensing and Modeling of Severe Weather (CETEMPS), L'Aquila, Italy, a Research Assistant with the Cooperative Institute for Research in Environmental Sciences (CIRES), University of Colorado, Boulder, CO, USA, an Adjunct Professor with the Department of Electrical and Computer Engineering, University of Colorado. He has nearly 20 years of experience with ground- and satellite-based passive remote sensing, particularly microwave radiometry. He has coauthored more than 80 peer-reviewed papers.

Dr. Cimini has been an Associate Editor for *Atmospheric Measurement Techniques* (European Geosciences Union) since 2013 and Remote Sensing (MDPI) since 2018. He was the recipient of the Fondazione Ugo Bordoni Award in 2008 in memory of Prof. G. D'Auria, and the 6th Hans Liebe Lectureship bestowed by the U.S. National Committee for the Union of Radio Scientists Internationale in 2019. He is a Life Member of the European Geosciences Union.

Elisabetta Ricciardelli received the M.S. degree in physics from the University of Bologna, Bologna, Italy, in 1998 and the Ph.D. degree in methods and technologies for environmental monitoring from the University of Basilicata, Potenza, Italy, in 2008.

In 2005, she was with the Institute of Methodologies for Environmental Analysis, Tito Scalo, Italy. Her research interests include satellite-data handling for meteorological studies with particular focus on cloud detection and classification.

Francesco Di Paola received the M.S. degree in physics from Sapienza University, Rome, Italy, in 2004 and the Ph.D. degree in geophysics from University Alma Mater Studiorum, Bologna, Italy, in 2008.

Since 2005, he has been a Researcher with the Italian National Research Council, Tito Scalo, Italy, and in 2011, he was with the Institute of Methodologies for Environmental Analysis, Tito Scalo. His research interests include rainfall estimation and nowcasting with multisensor approach combining MW-IR satellite data with lightning data from surface networks.

Tim Hultberg has been a Remote Sensing Expert with EUMETSAT since 2013, working on IASI and IASI-NG science and applications.

Thomas August received the M.Sc. degree in astrophysics and planetology from the University of Toulouse, Toulouse, France, in 1997 and the Ph.D. degree in astrophysics from the University of Bordeaux, Talence, France, in 2002 (for a research work financed by Centre National dtudes Spatiales on the potential of synthetic aperture radars for the remote exploration of subsurfaces).

Since 2003, he has been with the European Organisation for the Exploitation of Meteorological Satellites, Darmstadt, Germany, where he contributed to the prototyping, the development, and the validation of the infrared atmospheric sounding interferometer (IASI) Level 2 (L2) products processor. As a Remote Sensing Scientist, since 2010, he has been leading the IASI L2 team and resumed responsibility for the evolution of the L2 products. His research interests include the atmospheric infrared sounding and retrieval techniques for temperature and humidity profiles, the surface temperature and emissivity, the atmospheric composition, and the cloud detection.

Filomena Romano received the M.S. degree in physics from the University of Bologna, Bologna, Italy, in 1990.

In 1992, she was with the Institute of Methodologies for Environmental Analysis, Tito Scalo, Italy, where she got experience on experimental and theoretical studies in atmospheric remote sensing. She collaborated in studies concerning retrieval of atmospheric aerosol from solar spectra at ground level. She has currently specialized in satellite data handling for meteorological and climatological studies. Her main research interests include cloud detection, cloud clearing, and cloud microphysical retrieval of infrared and microwave radiance from space-borne sensors.